Chem Rev Lett 9 (2026) 169-178

Research Article

Chemical Review and Letters
journal homepage: www.chemrevlett.com
ISSN (online): 2645-4947 (print) 2676-7279

DFT calculations of structural, elastic, electronic and optical properties of $CaXH_3$ (X= Co, Rh)

Abdellah Elkaiem[1,*], Omar Boukraa[1,2]

[1]*Faculty of Mathematics and Material Sciences, University of Ouargla, Ouargla 30000, Algeria.*
[2]*Laboratory for the Development of New and Renewable Energies in Arid and Saharan Zones, Ouargla 30000, Algeria.*

ARTICLE INFO

Article history:
Received 23 June 2025
Received in revised form 13 August 2025
Accepted 19 August 2025

Keywords:
Density functional theory
WIEN2K code
$CaXH_3$ hydrides
Electronic
Elastic

ABSTRACT

Structural, elastic, electronic and optical properties of the perovskite-type hydrides $CaXH_3$ (X = Co, Rh) were investigated using the first-principles full-potential linearized augmented plane wave method based on density functional theory calculations. We have investigated formation energies, lattice parameters, bulk moduli, elastic constants, electronic structures, and optical properties. Calculated negative formation energies point to their stability, and indicate that the most stable compound is $CaRhH_3$. In addition, elastic properties and mechanical coefficients confirm that these compounds are stable. The densities of states (DOS) in the compounds are not zero at the Fermi level reflecting their metallic behavior and the largest contributions to the partial DOS'es were observed to stem from the presence of the transition metal element. The hybridization reaction between X-d states and H-1s states is stronger than that between Ca-d states and H-1s states, which is an important feature for these hydrogen storage compounds.

1. Introduction

Laptops and mobile phones rely on portable power sources and long battery life is an important point for these devices. In addition to these electronic devices, portable power sources are required for entertainment activities, military applications, education, etc. [1]. Currently, modern batteries are the most widely used portable power sources which have limitations such as capacity. Another portable power source is fuel cell and hydrogen fuel cell [2]. The formation of $CaRhH_3$, a perovskite hydride, is achieved from the Laves phase $CaRh_2$ by hydrogenation. Initially, $CaRh_2$ forms successive Laves phase hydrides, then, at high temperature and pressure, transforms into nanocrystalline rhodium and $CaRhH_3$. Initial phase: $CaRh_2$ (Laves phase): $CaRh_2$, a cubic Laves phase, is the starting point. Under hydrogen pressure and at room temperature, $CaRh_2$ hydrogenates to form Laves phase hydrides. Three hydrides are successively formed: α-$CaRh_2H_{0.05}$, β-$CaRh2D_{3.93}$, and γ-$CaRh_2D_{3.2}$. By increasing the temperature and pressure (560 K and 5 MPa), the hydrided Laves phase transforms. This transformation leads to the formation of nanocrystalline rhodium and $CaRhH_3$, a perovskite-type hydride. $CaRhH_3$ can be synthesized in this way, as it is not easily accessible by other methods. In summary, the formation of $CaRhH_3$ involves a two-step reaction: the progressive hydrogenation of the Laves phase $CaRh_2$, followed by its transformation into $CaRhD_{2.93}$ and rhodium under higher temperature and pressure conditions [3-4]. In 2006, Ikeda *et al* [5] determined X-ray diffraction profiles of $CaXH_3$ for the transition metal series (X = Ti, V, Cr, Mn, Fe, Co, Ni and Cu) after mechanical milling and indicated that cubic perovskite type hydrides (space group 221) can be formed for X = Co, Fe and Ni, but not for X = Ti, V, Cr, Mn, and Cu. The general observation is that the geometric Goldschmidt tolerance factor *t*, which can be calculated for a known crystal structure, lies in the interval 0.9-1.0 for stoichiometric ABH_3 compounds. However, in 2008, Ikeda et al [6] advanced that if the hydrogen concentration is less than the perovskite stoichiometric composition AXH_3,such as in the cases of $CaPdH_2$, $SrPdH_{2.7}$, and $YbPdH_{2.7}$, the values of the Goldschmidt tolerance factor *t* tends to be smaller than 0.9. By calculating the tolerance factor for $CaCoH_3$, one finds $t = 0.9$ and yet this hydride is known to have a cubic perovskite type structure as mentioned by [6]. Since material synthesis synthesis is a very time consuming effort, there is a need for a materials specific theory with

* Corresponding author E-mail: kaim.a.allah@gmail.com
https://doi.org/10.22034/crl.2025.531066.1635

a predictive power for the Formation Energy At present the state of the art is formed by first principles calculations based upon Density Functional Theory (DFT). Several papers have been dedicated to trends in the DFT Fees of hydrides (alanates and boranates [7,8]. In this work, we propose to investigate the two compounds $CaCoH_3$ and $CaRhH_3$ from the point of view of their stability, structure, elastic, electronic, and optical properties by using ab initio calculations based on density functional theory (DFT).

2. Materials and Methods

Our calculations have been performed using the full-potential linearized augmented plane wave (FP-LAPW) [9] method based on the density functional theory (DFT), [10] as implemented in the WIEN2k code the exchange correlation interaction was treated approximated by the generalized gradient approximation (GGA 96) as proposed by Perdewe-Broukee-Ernzerhof [11] the Kohne Sham equations are solved self-consistently by choosing the muffin-tin radii (MT) to be 2.5 a.u for Ca and to be 2 for Co, Rh and 1.2 for H ,We computed E(Ry) by changing $R_{mt}.K_{max}$ and the number of k-points in order to optimize these parameters so that they allow the calculation of the stable structure and its properties in an acceptable time.

3. Results and Discussion

3.1. Hydrogen storage properties

This work aims to predict novel classes of perovskite hydrogen storage compounds such as $CaCoH_3$ and $CaRhH_3$ with reasonable gravimetric hydrogen densities C_{wt} (in %) calculated using:

$$C_{wt} = \frac{1}{1+\frac{1M_M}{xM_H}}, \quad (1)$$

where M_H is the molar mass of hydrogen, M_M that of the entire host material (without hydrogen), and x the hydrogen to metal ratio [12]. This shows that, when the atomic mass of the X element increases, gravimetric hydrogen storage capacities decrease due to an increase in the mass of the whole hydride. Lattice constants increase as the atomic number of the X(Co, Rh) element increases This contradicts what was stated in Reference [13] and agrees with Reference [14]. The gravimetric hydrogen densities of both compounds are found to be 2.97 and 2.07 for $CaCoH_3$ and $CaRhH_3$, respectively these calculated values are less than compared to $Mg2FeH_6$ and $NaAlH_4$ compounds are 5.47, 5.5 respectively [15, 16]. The mass densities ρ of the compounds are calculated by using relation (2) and investigated by the IRelast package as implemented in WIEN2k.

$$\rho = \frac{ZM}{a^3 N_a} \quad (2)$$

where Z is the number of atoms in a unit cell, M is the molar mass of the compound, a is the lattice constant, and N_a Avogadro's number. $CaRhH_3$ has a lower gravimetric storage density than $CaCoH_3$.In the literature, the gravimetric hydrogen storage capacities of both $CaXH_3$(X= Co, Rh) compounds are lower than those calculated for $NaXH_3$ (X = Mn, Fe, Co)[17]. It is also noted that as the lattice parameter of the compound increases, the atomic number of (X = Co, Rh) increases, and this is the opposite of what was stated in Reference [13]. This is due to the presence of the two elements Co and Rh in the same column of the periodic table, while the elements Co, Fe and Mn are located in the same line of the periodic table while our results are consistent with what was stated in Reference [14].

3.2. Structural properties

We have optimized the structural parameters for $CaCoH_3$ and $CaRhH_3$ by fixing the experimental atomic position and varying the cell volume by ±9, ±7, ±5, ±3, ±1 and 0 % of the experimental volume ; and we have calculated total energy versus volume we have optimized both compounds , structure and calculated the total energy as function of unit cell volume . The unit cell of $CaXH_3$ (X = Co, Rh), having a perovskite structure and a space group Pm3m (no. 221), is depicted in Figure 1. where Co atoms are placed at the cube center (1/2, 1/2, 1/2), calcium (Ca) atoms are positioned at the corners (0, 0, 0) and hydrogen (H) atoms are located at the face centers (1/2, 1/2, 0)[18], while in $CaRhH_3$ is depicted Ca atoms are placed at the cube center (1/2, 1/2, 1/2), calcium (Rh) atoms are positioned at the corners (0, 0, 0) and hydrogen (H) atoms are located at the face centers (1/2, 1/2, 0)[3]. The structures are optimized for both compounds by computing their cell total energy versus its volume, then fitting the calculated points to Murnaghan's equation of state in order to extract equilibrium lattice constants (a) and bulk moduli (B). These parameters are presented in Table 2. In addition, the stabilities of the materials have been verified by calculating their total energies. Obtained values are -4151.40 Ry.

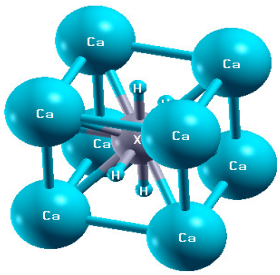

Fig. 1. Unit cell of $CaXH_3$ (X = Co, Rh)

3.3. Hydride formation energies

Storage of hydrogen in metal hydrides is possible since many metals react easily with hydrogen forming a

stable metal hydride formation energies are a significant methods to determine if the predicted phased are likely to be stable for that to verifying order to see if either compound has the ability for stability formation enthalpies of $CaXH_3$, which are calculated by using the formula 3 below, are all negative reflecting the stability of these hydrides In theory, for example from [19], the formation of a $CaXH_3$ compound can be accomplished from its primary elements according to the following reaction: $Ca + X + 3/2\ H_2 \rightarrow CaXH_3$. As a case in point, for rhodium:

$$\Delta H_f(CaRhH_3) = E_{tot}(CaRhH_3) - [E_{tot}(Ca) + E_{tot}(Rh) + 3/2E_{tot}(H_2)] \quad (3)$$

where $E_{tot}(CaRhH_3)$ symbolizes the total energy of $CaRhH_3$ and $E_{tot}(Ca)$, $E_{tot}(Rh)$,and $E_{tot}(H_2)$are the ground state energies for one Ca atom, one Rh atom, and one H_2 molecule, respectively It should be noted that some authors calculated the formation energies of $MgXH_3$ compounds starting, not from the elements, but from MgX [20], according to the following formula:

$$\Delta H_f(MgXH_3) = E_{tot}(MgXH_3) - [E_{tot}(MgX) + 3/2E_{tot}(H_2)] \quad (4)$$

We calculated the total energy for Ca, Rh and adopted that published in the literature for the H_2 molecule which is $E_{tot}(H_2)$=-2.32Ry [21, 22].

The total energy for the Co atom taken in our calculations was found to be -2786.95Ry in [23]. The computed negative formation enthalpies according to eq. (3) are listed in Table 1 and Figure 2.

3.4. Desorption temperatures

$CaCoH_3$ has a high thermodynamic stability due to its high formation enthalpy ΔH =73.32 kJ/mol.H_2 also $CaRhH_3$ has a high thermodynamic stability due to its high formation enthalpy ΔH =89.94 kJ/mol.

H_2 formation energy are used to estimate the desorption temperature of the studied compounds according to the following equation (5) [20]:

$$\Delta H = T\Delta S \quad (5)$$

Where, the variation of the entropy is taken at standard pressure and temperature to be equal [20]:

$$\Delta H \approx \Delta S(H_2) = 130\ \mathrm{J/mol.K} \quad (6)$$

The results calculated by relation 6 show that $CaCoH_3$ has a high desorption temperature of order 543.46 K. also $CaRhH_3$ has a high desorption temperature of order 672.84 K This prevents their application for mobile hydrogen storage.

Table 1. Lattice constant *a(Å)*, atomic positions, bulk modulus *B(GPa)*, pressure derivative *B_0'(GPa)* of bulk modulus , total energy E(Ry), and formation energies ΔH_f of $CaXH_3$ compounds.

Compounds	Lattice constant (Å)	Atomic positions $CaXH_3$ (X = Co, Rh)	*B*	*B_0'*	Total energy E (Ry)	Formation energies ΔH_f
$CaCoH_3$	*a*=3.55[a] *a*=3.52[b] *a*=3.48[c] *a*=3.49 (present)	Ca:0,0,0 [a] X:0.5,0.5,0.5 H: 0.5,0.5,0	105 (present) 105 [c]	5.99	-4151.40	-0.54Ry -71.03Kj/mol.H_2
$CaRhH_3$	*a*=3.64[d] *a*=3.66 (present)	Ca:0.5,0.5,0.5 [d] X:0,0,0 H: 0.5,0.5,0	101.66	3.81	-10935.011	-0.66Ry -87.94 Kj/mol.H_2

[a] [5] Experimental. [b] [18] Experimental. [c] [13] GGA by VASP. [d] [3] Experimental

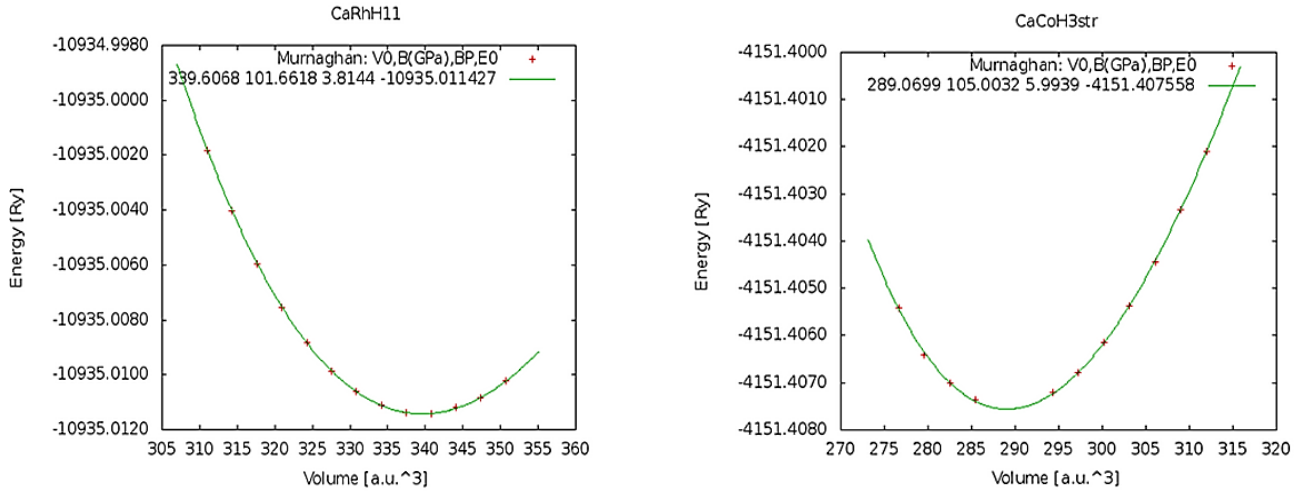

Fig. 2. Total energy as a function of volume for $CaRhH_3$ and $CaCoH_3$ respectively by the GGA-DFT method

3.5. Elastic properties

Elastic constants are calculated to investigate the mechanical properties of $CaXH_3$(X=Co, Rh) compounds, as elastic constants play an important role in determining the nature of binding forces and mechanical stabilities, In this work, elastic constants are investigated by the IRelast package as implemented in WIEN2k [24] Born stability criteria for cubic crystals are given as [25]:

$$C_{11} - C_{12} > 0, C_{11} > 0, C_{44} > 0, C_{11} + 2C_{12} > 0$$

By using the Voigt-Reuss-Hill approximations Obtained by the IRelast package in GGA method which can be calculated and verified by the following relationships [26]:

$$B = \frac{(C_{11}+2C_{12})}{3} \quad (7)$$

$$E = \frac{9BG_V}{3B} + G_V \quad (8)$$

$$G = 1/2\,(G_V + G_R) \quad (9)$$

By the IRelast package The bulk, shear and Young's moduli have been determined with the Voigt (G_V), Reuss (G_R) and Hill approximations. where we report in Table 2 the average value from these three approximations also The calculated elastic constants (C_{ij}) for the both compounds have been reported in Table 2 and where the adequate constants are C_{11}, C_{12} and C_{44} for the cubic structures. It can be concluded from the values that both compounds are stable and satisfying the Born stability criteria given above .

Shear constants have also been calculated to assess the dynamic stability by using the following formula C' = ($C_{11} - C_{12}$)/2 [26]. Table 2 show that the shear constant is positive for both compounds, corroborating the stability of both compounds.

to check the bonding nature in the compounds, Cauchy pressure (C_p) calculated from the relation C_{12} - C_{44} have also been listed in Table 2 ,The negative Cauchy pressure value indicates the brittleness while the positive indicates the ductility [27], we found $CaCoH_3$ compound have negative Cauchy pressure indicating that studied the compound is brittle material. This brittleness property similar to $NaMgH_3$, $NaCoH_3$,$NaMnH_3$ [17], while $CaRhH_3$ compound is ductile nature because have positive Cauchy pressure .

The B/G ratio, when greater than 1.75, points to ductility while it signals brittleness otherwise [13]. In our case, the B/G ratios reported in Table 2 confirm the ductile nature of $CaRhH_3$ and the brittle nature of $CaCoH_3$. The last parameter listed in the table is Poisson's ratio which is calculated from ν = (3B − 2G)(3B + G)/2. A value less than 0.24 [13] indicates covalent bonds for the $CaCoH_3$ compound whereas ionic bonding is favoured in $CaRhH_3$. Based on the Cauchy pressure and B/G for $CaRhH_3$, it can be said that this compound has a ductile nature. On the other hand, the $CaCoH_3$ compound have a negative value of Cauchy pressure and a B/G ratio less than 1.75, indicating a brittle character. In hydrogen storage applications, ductility and brittleness of materials is extremely important. Ductile materials will be easy to handle, especially for portable hydrogen storage applications; conversely, brittle materials will require extra caution. Consequently, it can be said that $CaRhH_3$ is the most suited material for this property [27].

The Debye temperature is linked to many physical properties such as specific heat, elastic constants, and melting point Debye temperatures can be calculated from the elastic constants, using the average sound velocity (v_m) with the following equation:

$$\theta_D = \frac{\hbar}{k_B}\left[\frac{3n}{4\pi}\left(\frac{N_A\rho}{M}\right)\right]^{1/3} v_m \quad (10)$$

where $\hbar$ is Planck's constant, k_B is Boltzmann's constant, ρ the volumic mass, n is the number of atoms in the molecule, N_A is Avogadro's number, and M is the molecular weight. Average sound velocities v_m can also be expressed in terms of transverse (v_t) and longitudinal (v_l) elastic wave velocities by using the following formula:

$$\frac{3}{v_m^3} = \frac{2}{v_T^3} + \frac{1}{v_L^3} \quad (11)$$

as given by Navier's equation [28]. Furthermore, transverse wave velocity v_t and longitudinal wave velocity v_l can be calculated by using G and B values as $v_t = (G/\rho)^{1/2}$ and $v_l = ((3B/4G)/\rho)^{1/2}$, respectively [28]. The calculated Debye temperature along with v_m, v_l, and v_t are presented in Table 3. From the data of elastic constants, another fundamental thermodynamic factor listed in Table 3, the melting temperature, has also been determined for these perovskites utilizing equation (12) [14].

$$T_{melt} = [553K + (5.91K/GPa)C_{11}] \pm 300. \quad (12)$$

The longitudinal, transverse and mean wave velocities and Debye temperature are also listed in Table 3 $CaCoH_3$ has a higher Debye temperature than the $CaRhH_3$ compound, Debye temperatures correlate with melting temperatures, specific heats, etc. This means that the related materials have a high thermal conductivity and a high melting temperature. As Debye temperatures in a solid can be used to characterize the strength of covalent bonds(It is well known that Debye temperature is can be used to characterize the strength of covalent bonds in solids) [28], a Debye temperature indicates that $CaCoH_3$ has the strongest bond Also the calculated Debye temperature are less than the Debye temperature of $NaCoH_3$, $NaMnH_3$, $NaFeH_3$ [17], and $CaFeH_3$, $CaCoH_3$, $CaMnH_3$ [13], the latter authors observing an increase of the Debye temperature with the decrease of lattice constants for all their compounds [17]. We also notice that the Debye temperature of both compounds is higher than that of the KBH_4 [29].

Table 2. Calculated elastic constants(C_{ij} *in GPa*), Cauchy pressure (C_p*in GPa*), shear constant (*C' inGPa*), bulk modulus (*B in GPa*),shear modulus (*G inGPa*),Young's modulus (*E in GPa*), *B/G* ratio, and Poisson's ratio of $CaXH_3$.

Compounds	C_{11}	C_{12}	C_{44}	C_p	C'	B	G	E	B/G	v
$CaCoH_3$	180.15	56.84	65.4	-8.56[a] -9.95[b]	57.35	97.94[a] 105[b]	63.87	157.41	1.53	0.23
$CaRhH_3$	166.63	52.45	37.89	14.56	57.09	90.51	44.67	115.08	2.03	0.29

[a] present. [b] [13] GGA by VASP code

Table 3. Transverse wave velocity v_T (*m/s*), longitudinal wave velocity v_L (*m/s*), average wave velocity v_m (*m/s*), Debye temperature θ_D (*K*), and melting temperature T_{melt} *(K)* of $CaXH_3$.

Compounds	v_T(m/s)	v_L(m/s)	v_m(m/s)	θ_D (K)	T_{melt}(K)
$CaCoH_3$	4174.84[a] 4130[b]	7068.5[a] 6991[b]	4625.34[a] 4576[b]	656[a] 669.36[b]	1617.70[a] 1617.68[c]
$CaRhH_3$	3081.87[a]	5648.57[a]	3437.23[a]	470.2[a]	1537.78[a] 1537.78[c]

[a] Calculated by the IRelast package of WIEN2k (present work). [b] [13] GGA by VASP code. [c] Calculated by equation (10)

3.6. Electronic structure calculations

3.6.1. Band structure

In Figure 3 and 4, the band structure of $CaCoH_3$ and $CaRhH_3$ is drawn in the R-∇-Γ-Δ-X-Z-M-Γ symmetry path. the R-Γ and M-Γ directions, the Fermi level is crossed In five points by an electron level that belongs to the d orbital of the Co and Rh atoms, the high density of levels on the sides of the Fermi surface, as well as the overlap and gradient of the levels in the conduction region.

As seen in Figure 3 and 4 there is no forbidden energy gap at the Fermi level for both compounds. In other words, the conduction and valence bands overlap with each other at the Fermi level. Thus, one can conclude that $CaXH_3$ (X=Co, Rh) compounds show a metallic character [27].

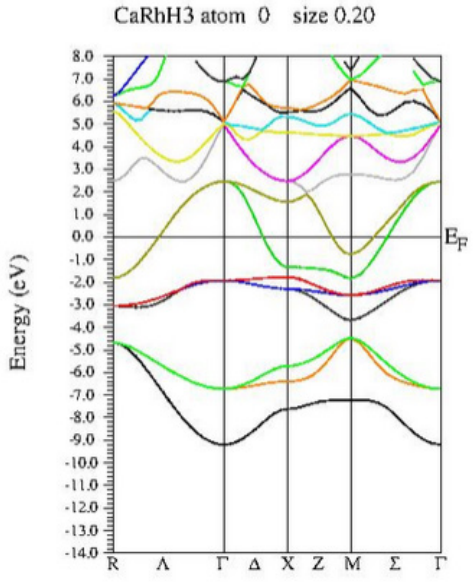

Fig. 3. Band structure of $CaRhH_3$ by using GGA.

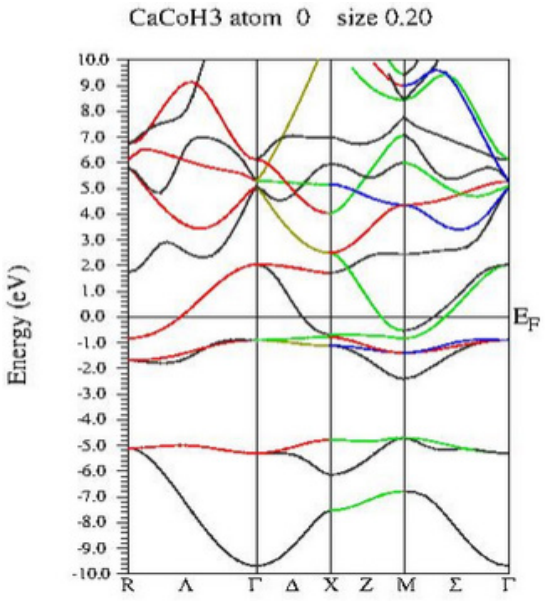

Fig. 4. Band structure of $CaCoH_3$ by using GGA.

3.6.2. The density of states

To explain the corresponding electronic properties of $CaCoH_3$ and $CaRhH_3$ compounds, the total density of states and partial density of states have been computed and are represented in Figure 5 and 6.the studied quantities are presented in the energy range -10 eV to 10 eV. It is clear from these figures that $CaCoH_3$ and $CaRhH_3$ have metallic behavior, the dominant contributions in the total DOS being related to pd-states of Ca, d-states of X (X = Co and Rh) and s-states of H. three distinct dispersion regions are specified in the valence bands for the studied compounds due to the contributions between the included states. The first region lies between -6 and -4.7 eV approximately for $CaCoH_3$ (between -8 and -4.5 eV for $CaRhH_3$).The density of state It is due to the hybridization of the X-d states with the H-s states whereas the second region is

comprised between -2.35 and 2 eV approximately for $CaCoH_3$ (between -3.6 and 2 eV for $CaRhH_3$), and is due to the hybridization of the X-d states and Ca-d states These bands are crossing the Fermi level to the conduction band, and the main contributions in the conduction band is due to Ca-d and X-d states.

The hybridization reaction between the X-d states and H-1s states is stronger than between Ca-d states and H-1s statesand this is a very important feature for the hydrogen storage aptitude of these compounds [13,14].

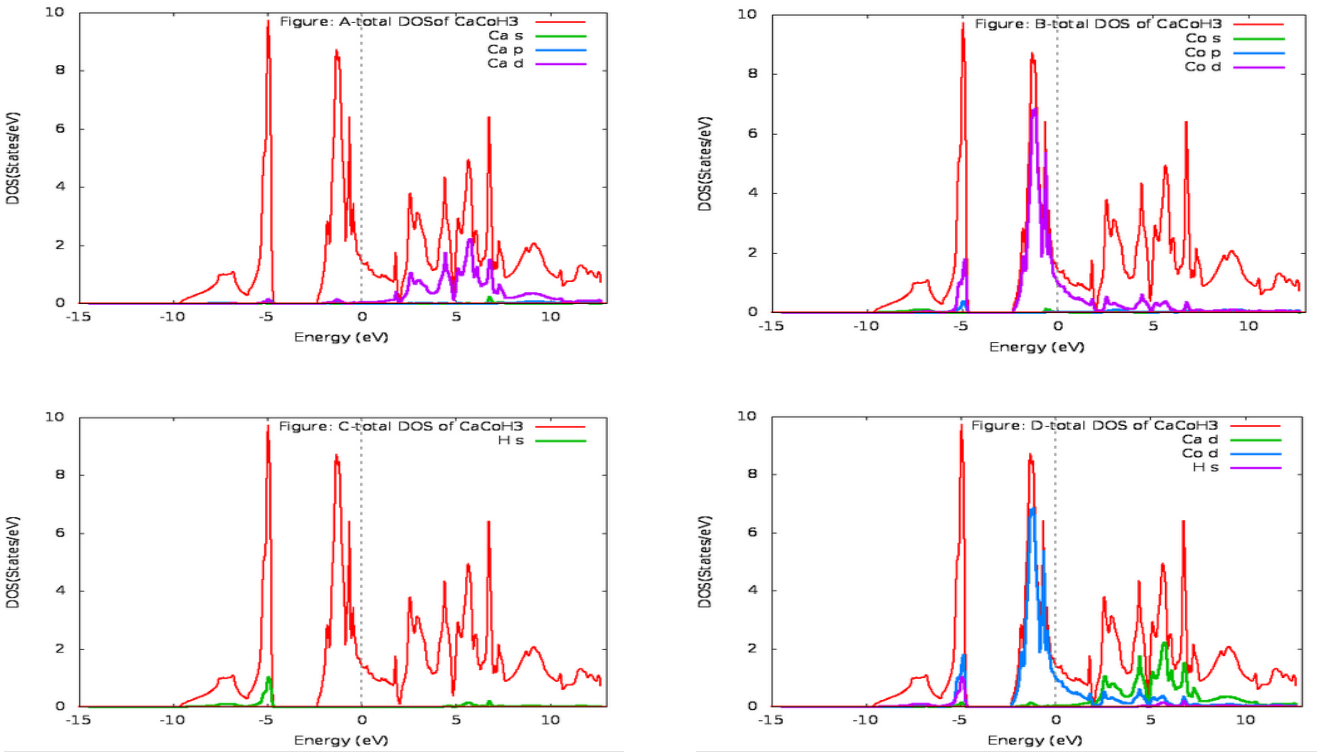

Fig. 5. Total and partial DOS for $CaCoH_3$ by using GGA.

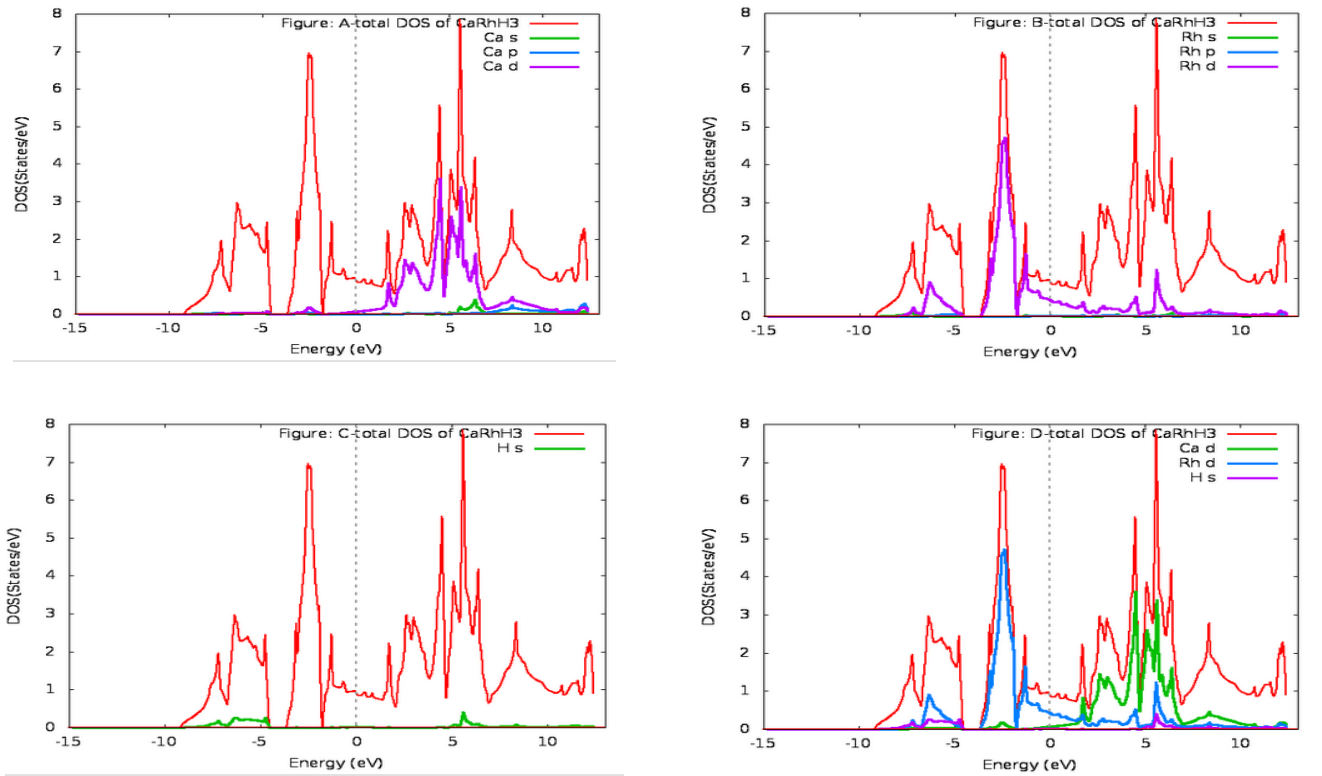

Fig. 6. Total and partial DOS for $CaRhH_3$ by using GGA.

3.7. Optical properties

We propose to investigate the following optical coefficients: the dielectric function ,the refractive index n(ω), the extinction coefficient , the absorption coefficient , the reflectivity , and the optical conductivity .Optical properties are related to electronic properties of the solid compound.The behavior of the main peaks in the optical spectra can be explained in terms of interband transitions from the valence band to the conduction band.The optical parameters can be described by the dielectric function ε(ω). This function is a fundamental complex quantity defined as [29, 30]:

(13)

The real and imaginary the parts of the dielectric function for $CaXH_3$ (X=Co, Rh) compounds are represented in Figure 7a, b respectively. The optical spectra of $CaXH_3$ have similar appearances since the conduction bands of these compounds have a similar character. The spectrum of , which is the sum of the band contributions from the valence and conduction bands, shows the absorption behavior of the compounds as obtained from the electronic band structure [14]. The calculated zero frequency values $\varepsilon_2(0)$ for $CaCoH_3$ and $CaRhH_3$ are 1.5 and 0.5, respectively.$\varepsilon_2(\omega)$ spectra increase sharply from these values, giving rise to the first peak located around 0.5 eV and 1.1 eV for $CaCoH_3$ and $CaRhH_3$, respectively. This peak is due to the electron transition from the X-d state and H-s state of the valence band to these states in the conduction band. Then the spectra attain several peaks while fluctuating. The second and third peaks represent the contribution of X-d and H-s states in the valence band to Ca-d, X-d and H-s states in the conduction band. The lowest peak on $\varepsilon_2(\omega)$ located around 11.8 eV is due to the electron transition from Ca-p state in the valence band to Ca-d, X-d and H-s states in the conduction band.

The real part of the dielectric function is obtained from $\varepsilon_2(\omega)$ using the Kramers-Kroning relationship [31]. The zero-frequency limit ε1(0) of $CaCoH_3$ ($\varepsilon_1(0)$= 12.2) is found larger than that calculated for $CaRhH_3$ ($\varepsilon_1(0)$ = 9.1). These values are found to be larger than those for semiconductor materials $KMgH_3$ and $MBeH_3$ (M = Li, Na and K), $\varepsilon_1(\omega)$ curve increases slightly to reach its maximum value of 13 around 0.48eV and 11 around 0.8 eV for $CaCoH_3$ and $CaRhH_3$ respectively. Then, the curve decreases sharply and keeps fluctuating while decreasing. It attains its negative value around 8.25 for $CaCoH_3$ and 9.3 for $CaRhH_3$, succeeded by an increase toward the zero value In the energy intervals where $\varepsilon_1(\omega)$ is negative .
as shown in Figure 7c. The calculated static refractive index (n(0)) value is found around 3.5 and 3 for $CaCoH_3$ and $CaRhH_3$, respectively These calculated values are higher compared to the calculated one for ZnO,and $KMgH_3$ which is 2.14 and 1.93 [32, 33] and approach those of $CaNiH_3$ and $CaPdH_3$ The maximum calculated value of n(ω) is found to be 3.7 around 0.2 eV for $CaCoH_3$ and 3.3 around 0.75eV for $CaRhH_3$.
The extinction coefficient k(ω) is represented in Figure 7d. Its maximum value is found 2.2 at 8.2 eV and 2.1 at 9.4 eV for $CaCoH_3$ and $CaRhH_3$,respectively.These values correspond to the zero value of $\varepsilon_1(\omega)$.

The absorption coefficient, I(ω), curve plotted in Figure 8f, shows clearly that both compounds have a high ability to absorb the electromagnetic radiation. The curve reaches its first maximum local value of absorption $177\times10^4 cm^{-1}$ around 8.2 eV for $CaCoH_3$ and $190\times10^4 cm^{-1}$ around 9.2 eV for $CaRhH_3$. The I(ω) spectrum is fluctuating and reaches its second $168.75\times10^4 cm^{-1}$ and 161.5 $\times10^4 cm^{-1}$ at energy levels around 9.4 eV and 10.7 eV for $CaCoH_3$ and $CaRhH_3$, respectively. As shown in I(ω) spectra, both compounds possess high ultraviolet absorption within the low energy range 7.5–13.5 eV.

The refractive index R(ω) spectrum is shown in Figure. 8e for both compounds studied. The zero-frequency R(0) value is about 30% and 25% for $CaCoH_3$ and $CaRhH_3$, respectively the spectrum reaches a maximum reflectivity of 45% at 8.25 eV for $CaCoH_3$ and 47% at 9.5 eV for $CaRhH_3$. These values are higher than those calculated for ZnO, and $KMgH_3$ [34, 35] which in ultraviolet region(10nm-400nm) as reported in Ref [32] therefore, both compounds can be considered UV-protected.
TiO_2 has a reflectivity of up to 100% at 10 ev, which is greater than the reflectivity of $CaCoH_3$ and $CaRhH_3$, which does not exceed 47% [36].

The energy loss function L(ω) spectrum is shown in Figure 8h this spectrum characterizes the energy loss of the fast electron crossing the compounds there is a distinctive peak appearing in the spectrum that describes the Plasmon peak. These peaks are associated with those for R(ω). The calculated Plasmon peak value is 0.63 and 0.5 located at plasma frequency of 11.5 eV and 12.5 eV for $CaCoH_3$ and $CaRhH_3$, respectively. At this energy value, the $\varepsilon_1(\omega)$ spectra for both compounds converge to zero.

The effective number of electrons, N(ω), is calculated using the sum rule [37]. From its curve in Figure 9I, N(ω) is null up to 1.5 eV for both compounds. Then, its value increases for $CaCoH_3$ and $CaRhH_3$.

The electrons conduction due to an applied electromagnetic field is expressed by the optical conductivity σ(ω). Its spectra are shown in Figure 8g, for the both studied compounds,the spectra have maximum values of 9500 $\Omega^{-1}cm^{-1}$ around 8 eV for $CaCoH_3$ and 8000 $\Omega^{-1}cm^{-1}$ around 9.25 eV for $CaRhH_3$.(the optical conductivity value of $CaRhH_3$ is similar of $CaNiH_3$) [14].

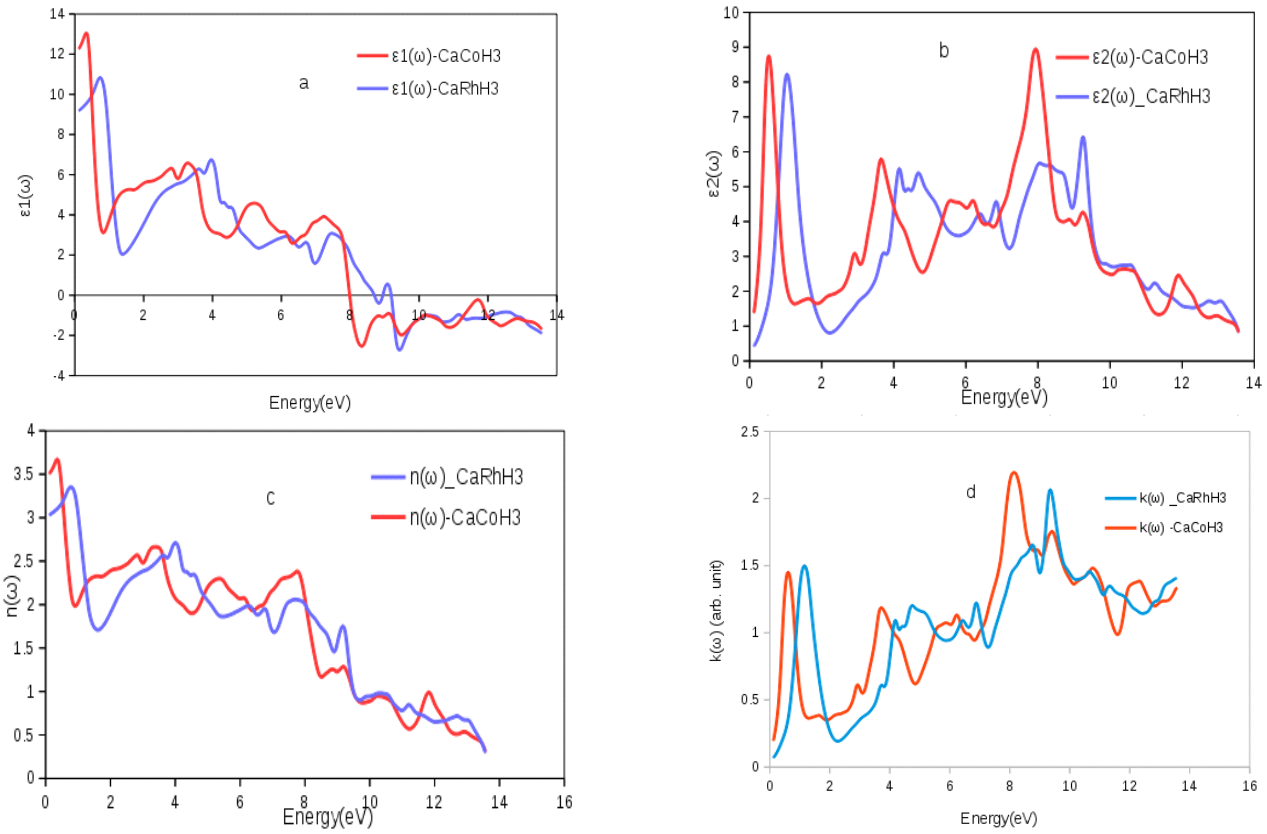

Fig. 7. Calculated (a) real $\varepsilon_1(\omega)$ and (b) imaginary $\varepsilon_2(\omega)$ parts of the dielectric function, (c) refractive index n(ω), (d) extinction coefficient k(ω), for the $CaCoH_3$ and $CaRhH_3$ compounds

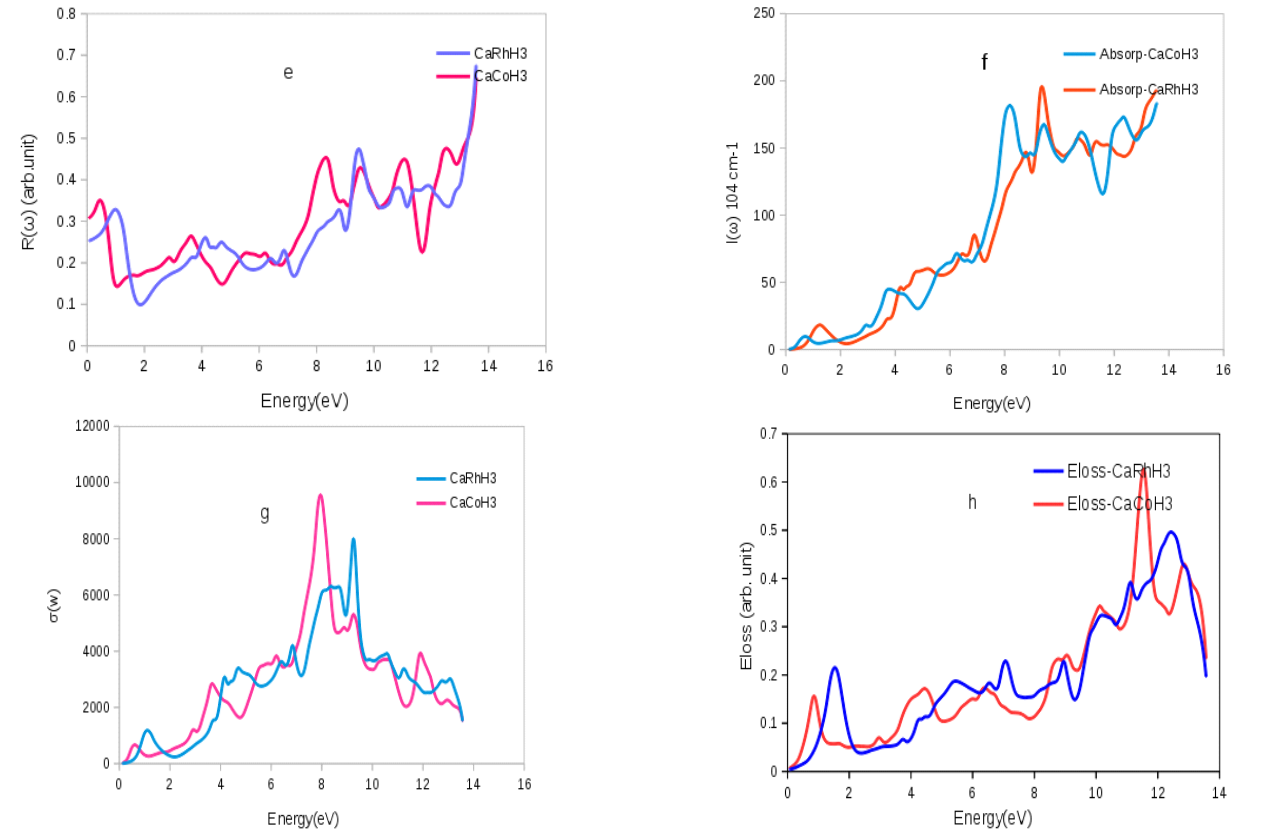

Fig. 8. Calculated optical properties (e) reflectivity R(ω), (f) absorption spectrum I(ω), and (g) optical conductivity σ(ω), (h) energy loss function for the $CaCoH_3$ and $CaRhH_3$ compounds.

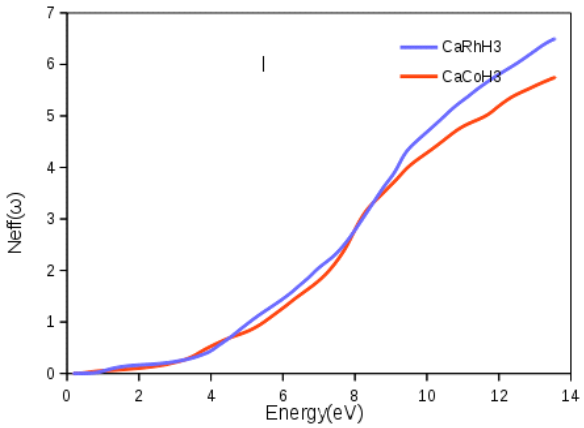

Fig. 9. Calculated optical properties : (I) sum rule $N_{eff}(\omega)$ for the $CaCoH_3$ and $CaRhH_3$ compounds.

4. Conclusion

The study of the structural properties of $CaXH_3$ (X = Co, Rh) compounds by the GGA method shows that the most stable compound is $CaRhH_3$ We find that both compounds crystallize in a cubic symmetry and calculated negative formation energies point to the stability of both compounds. In addition, determined bulk moduli, and other mechanical parameters, indicate their mechanical stability. Mechanical stabilities of both compounds are evaluated using elastic constants. It is found that both compounds fulfill the well-known Born mechanical stability condition. We discern the best compound for storing hydrogen among our studied compounds as $CaRhH_3$ by calculating a positive Cauchy pressure. By computing the gravimetric hydrogen storage capacities for potential hydrogen storage applications, we find that both compounds have suitable values.

The densities of states and band structures show that both compounds are metals Upon studying the electronic properties, we find that the d-band of transition elements hybridize with the s-band of hydrogen leading to the main bonds and orbits controlling the stability of both compounds. These revealed properties of $CaXH_3$ (X = Co, Rh) compounds may open new scopes for researchers to investigate their possible hydrogen storage applications. By studying the optical properties, we found that the two compounds have important optical properties may also be beneficial in the quest for new hydrogen storage applications

References

[1] T. Wilberforce, A. Alaswad, A. Palumbo, M. Dassisti, Advances in stationary and portable fuel cell applications. *Int. J. Hydrogen Energy*, 41 (2016) 16509.

[2] P. Ferreira, A. Paricio, A.M. Chaparro, Portable hydrogen energy systems: fuel cells and storage fundamentals and applications, (2023).

[3] A. Götze, J. Möllmer, H. Kohlmann, From the Laves Phase CaRh2 to the Perovskite CaRhH3: In Situ Investigation of Hydrogenation Intermediates CaRh2Hx. *Inorg. Chem.*, 57 (2018). DOI:10.1021/acs.inorgchem.8b01547.

[4] K. Spektor, W.A. Crichton, S. Filippov, J. Klarbring, S.I. Simak, A. Fischer, et al., Na−Ni−H Phase Formation at High Pressures and High Temperatures: Hydrido Complexes [NiH5]3− Versus the Perovskite NaNiH3. *ACS Omega*, 5 (2020) 8730−8743.

[5] K. Ikeda, S. Kato, K. Ohoyama, Y. Nakamori, H.T. Takeshita, S. Orimo, Formation of perovskite-type hydrides and thermal desorption processes in Ca–T–H (T = 3d transition metals). *Scripta Mater.*, 55 (2006) 827.

[6] K. Ikeda, T. Sato, S. Orimo, Perovskite-type hydrides-synthesis, structures and properties. *Int. J. Mater. Res.*, 99 (2008) 471.

[7] Y. Nakamori, et al., Physical Review B. *Phys. Rev. B*, 74 (2006) 045126.

[8] P. Vajeeston, P. Ravindran, A. Kjekshus, H. Fjellvag, *J. Alloys Compd.*, 387 (2005) 97.

[9] P. Blaha, K. Schwarz, P. Sorantin, S.B. Trickey, *Comput. Phys. Commun.*, 59 (1990) 399.

[10] P. Hohenberg, W. Kohn, Inhomogeneous Electron Gas. *Phys. Rev.*, 136 (1964) B864.

[11] J.P. Perdew, K. Burke, M. Ernzerhof, Generalized Gradient Approximation Made Simple. *Phys. Rev. Lett.*, 77 (1996) 3865.

[12] a) C. Camirand, Étude de la chaleur spécifique et de la conductivité thermique des hydrures métalliques par calorimétrie différentielle (2000) (Thesis). b) F. Najafi, S.S. Alamdar, E. Vaziri, Fullerene (C20) as a Sensor for the Detection of Nordazepam: DFT Simulations. *J. Med. Med. Chem.*, 1 (2025) 18–23. c) N. Mirderikvand, M. Mahboubi-Rabbani, A DFT Study on Citalopram Adsorption on the Surface of B12N12. *J. Chem. Technol.*, 1 (2025) 90–95. d) F. Iorhuna, A.M. Ayuba, A.T. Nyijime, Comparative study of skimmianine as an adsorptive inhibitor on Al (110) and Fe (111) crystal surface, using DFT and simulation method. *J. Chem. Lett.*, 4 (2023) 148–155.

[13] G. Surucu, A. Gencer, A. Candan, H.H. Gullu, M. Isik, CaXH3 (X = Mn, Fe, Co) perovskite-type hydrides for hydrogen storage applications. *Int. J. Energy Res.*, 44 (2020) 2345.

[14] a) F. Hamioud, A.A. Mubarak, Structural, elastic and optoelectronic properties of the hydrogen based perovskite compounds: Ab-initio study. *Chin. J. Phys.*, 56 (2018) 1. b) R. Ahmadi, Furazolidone Adsorption on the Surface of

B12N12: DFT Simulations. *J. Med. Med. Chem.*, 1 (2025) 100–105.
[15] L. Silvestri, L. Farina, D. Meggiolaro, S. Panero, F. Padella, S. Brutti, et al., Reactivity of Sodium Alanates in Lithium Batteries. *J. Phys. Chem. C*, (2015).
[16] X. Zhang, W. Tian, J. Yang, R. Yang, J. Zheng, X. Li, Synthesis and Hydrogen Storage Behaviour of Pure Mg2 FeH6 at Nanoscale. *Mater. Trans.*, 52 (2011) 618.
[17] G. Surucu, A. Candan, A. Gencer, M. Isik, First-principle investigation for the hydrogen storage properties of NaXH3 (X= Mn, Fe, Co) perovskite type hydrides. *Int. J. Hydrogen Energy*, 44 (2019) 30218.
[18] H.T.L. Nguyen, Pressure-induced metallic phase of hydrogen-rich systems (Doctoral thesis, Osaka University, Japan: 2012).
[19] T. Sato, D. Noréus, H. Takeshita, U. Häussermann, Hydrides with the perovskite structure: General bonding and stability considerations and the new representative CaNiH3. *J. Solid State Chem.*, 178 (2005) 3381.
[20] M. Abdellaoui, M. Lakhal, H. Benzidi, O. Mounkachi, A. Benyoussef, A. El-Kenz, et al., The hydrogen storage properties of Mg-intermetallic-hydrides by ab initio calculations and kinetic Monte Carlo simulations. *Int. J. Hydrogen Energy*, 45 (2020) 11158.
[21] Y. Bouhadda, A. Rabehi, S. Bezzari-Tahar-Chaouche, First-principle calculation of MgH2 and LiH for hydrogen storage. *Rev. Energ. Renouv.*, 10 (2007) 545.
[22] L. Mohammedi, B. Daoudi, A. Boukraa, Ab-initio structural and electronic properties of the intermetallic compound TiFeH2. *Comput. Condens. Matter*, 2 (2015) 11-15.
[23] R. Riqne, A. Abdiche, L. Hamere, M. Guemmou, N. Ouaini, S.F., Ab initio investigations of the electronic and magnetic structures of CoH and CoH2. *Solid State Sci.*, 22 (2013) 77-81.
[24] M. Jamal, IRelast, (2014) http://www.wien2k.at.
[25] F. Mouhat, F.X. Coudert, Necessary and sufficient elastic stability conditions in various crystal systems. *Phys. Rev. B*, 90 (2014) 224104.
[26] G. Raza, H.H. Murtaza, Umm-e-Hani, N. Muhammad, S.M. Ramay, First-principle investigation of XSrH3 (X = K and Rb) perovskite-type hydrides for hydrogen storage. *Int. J. Quantum Chem.*, 120 (2020) e26419.
[27] S. Al, Investigations of Physical Properties of XTiH3 and Implications for Solid State Hydrogen Storage. *Z. Naturforsch. A*, 74 (2019) 1023.
[28] Y. Bouhadda, S. Djellab, M. Bououdina, Y. Boudouma, N. Fenineche, Structural and elastic properties of LiBH4 for hydrogen storage applications. *J. Alloys Compd.*, 534 (2012).
[29] X.D. Zhang, Z.F. Hou, Z.Y. Jiang, Y.Q. Hou, Elastic properties of MBH4 (M = Na, K, Rb, Cs). *Physica B*, 406 (2011) 2196–2199.
[30] P. Blaha, K. Schwarz, F. Tran, R. Laskowski, G.K.H. Madsen, L.D. Marks, WIEN2k: An APW+lo program for calculating the properties of solids. *J. Chem. Phys.*, 152 (2020) 074101.
[31] M. Fox, *Optical Properties of Solids*, Oxford University Press, (2010).
[32] A.H. Reshak, M.Y. Shalaginov, Y. Saeed, I.V. Kityk, S. Auluck, *J. Phys. Chem. B*, 115 (2011) 2836.
[33] A. Elkaiem, O. Boukraa, Contribution to the Development of Nano-Composite Materials Based on ZnO and Polymethyl Methacrylate Structural and Optical Study. *Iraqi J. Phys.*, 23 (2025) 12.
[34] M.A. Ghebouli, B. Ghebouli, A. Bouhemadou, M. Fatmi, S. Bin-Omran, Structural, elastic, electronic, optical and thermodynamic properties of KMgH3. *Solid State Sci.*, 13 (2011) 647–652.
[35] R. John, S. Padmavathi, Ab Initio Calculations on Structural, Electronic and Optical Properties of ZnO in Wurtzite Phase. *Cryst. Struct. Theory Appl.*, 5 (2016) 4-41.
[36] T. Mahmood, C. Cao, F.K. Butt, H. Jin, Z. Usman, W.S. Khan, et al., Elastic, electronic and optical properties of cotunnite TiO2 from first principles calculations. *Physica B*, 407 (2012) 4495–4501.
[37] D. Guendouz, Z. Charifi, H. Baaziz, T. Ghellab, N. Arikan, S. Uğur, et al., Electronic structure, optical and thermodynamic properties of ternary hydrides MBeH3 (M = Li, Na, and K). *Can. J. Phys.*, 94 (2016) 865–876.